

SIZE EFFECT IN PENETRATION OF SEA ICE PLATE WITH PART-THROUGH CRACKS. II: RESULTS

By Zdeněk P. Bažant,¹ Fellow, ASCE, and Jang Jay H. Kim²

ABSTRACT: After development of the theory in the part I paper, systems of up to 300 nonlinear equations are solved in this paper by the Levenberg-Marquardt optimization algorithm. The maximum load is reached when the circumferential cracks begin to form. Numerical calculations show a typical quasi brittle size effect such that the plot of $\log \sigma_N$ versus $\log h$ (where σ_N = nominal stress at maximum load and h = plate thickness) is a descending curve whose slope is negligible only for $h < 0.2$ m and then gets gradually steeper, asymptotically approaching $-1/2$. The calculated size effect agrees with the existing test data, and contradicts previous plasticity solutions.

INTRODUCTION

The part I paper (Bažant and Kim 1998) in this issue presented the theory of a numerical solution of the fracture problem of penetration of an object through a floating ice plate. The present paper will use the theory to obtain results on the size effect and compare them to experimental data. Broader issues of scaling will also be studied. All the notations and definitions from the part I paper will be retained.

NUMERICAL CALCULATION OF DEFLECTION, STRESS, AND CRACK DEPTH PROFILES

To study the vertical depth profile of the radial crack, the stress distributions and, most important, the size effect, ice plates with various thicknesses are analyzed numerically. The schematic picture of the part-through numerical analysis model of an ice plate is shown in Figs. 1 and 2 of part I. An ice plate with an angle of 60° between the radial cracks in a star pattern is chosen as the basic case to solve. This is the angle that was commonly observed in the field tests by Frankenstein (1963). Although his experiments were carried out on lake ice, it seems reasonable to assume that the wedge angle would be the same for sea ice.

Because the structure is symmetric with respect to any crack line and the centerline of any wedge, one needs to analyze only a half wedge, with a 30° central angle. The ice plate is assumed to have a fixed support on a circle of radius $3L$. This support is far enough from the applied load resultant to ensure that the region with the crack behaves almost as if the plate were infinite.

The vertical load is considered to be applied on the plate as a uniformly distributed load along the edge of a circular hole of radius $0.1L$, where L is the flexural wavelength of ice. This is done for the sake of convenience, to avoid dealing with the moment singularity that would occur if the load were concentrated. The behavior at the beginning of crack propagation is of course affected by the presence of the hole, but at radial distances that matter for the long crack at maximum load (which exceeds $0.2L$ for all L), the behavior is nearly the same as for a plate in which the load is either concentrated or applied uniformly over the area of the circle. This fact (which is

a manifestation of the Saint-Venant principle) justifies the assumed mode of loading. The reason that the radius of the hole is increased in proportion to L is to maintain strict geometric similarity, which makes it possible to obtain precise information on the size effect, free from the effects of shape (or geometry). The crack profiles are shown in Fig. 1.

The mechanical properties of sea ice vary widely (Sanderson 1988), depending on the type of ice, temperature, and salinity. In the present study, the following typical ice properties are assumed: $f'_t = 0.2$ MPa, $\nu = 0.29$, $E = 1.0$ GPa, and $K_c = 0.1$ MN $m^{-3/2}$ (Sanderson 1988), but some other values are also considered. The specific weight of water, $\rho = 9,810$ N/m³.

The mesh used to calculate the compliance matrices has 60 uniformly spaced angular nodes within one-half of the wedge and 100 nodes on the radial rays. The spacing of the nodes along the radial ray is dense near the hole and is getting gradually coarser farther away [Fig. 2 of part I]. The reason for

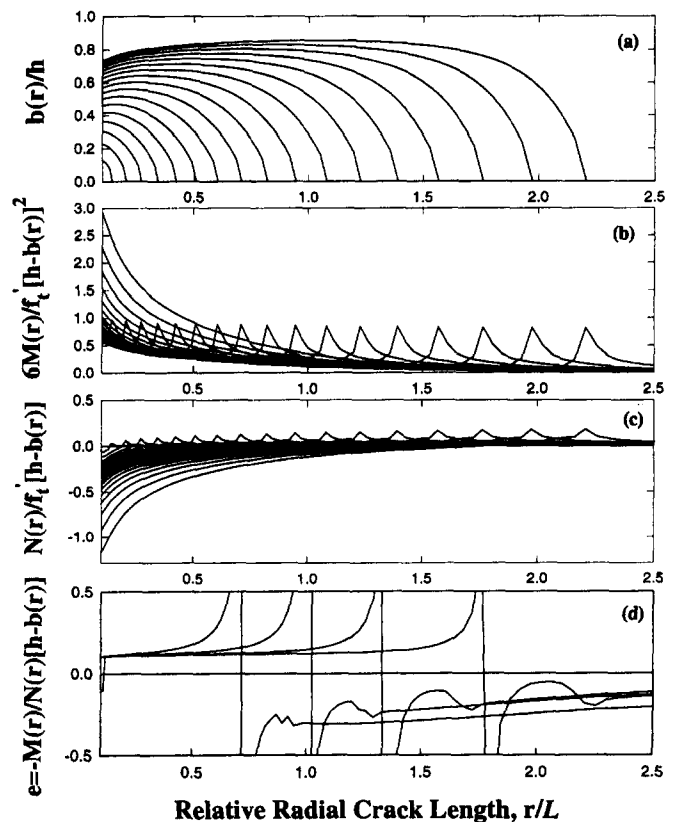


FIG. 1. Calculated Profiles of Nominal Stresses due to Bending Moment and Normal Force, Crack Depth Profiles, and Vertical Shift of Normal Stress Resultant

¹Walter P. Murphy Prof. of Civ. Engrg. and Mat. Sci., Northwestern Univ., Evanston, IL 60208. E-mail: z-bazant@nwu.edu

²Grad. Res. Asst., Dept. of Civ. Engrg., Northwestern Univ., Evanston, IL.

Note. Associate Editor: George V. Voyiadjis. Discussion open until May 1, 1999. Separate discussions should be submitted for the individual papers in this symposium. To extend the closing date one month, a written request must be filed with the ASCE Manager of Journals. The manuscript for this paper was submitted for review and possible publication on March 12, 1998. This paper is part of the *Journal of Engineering Mechanics*, Vol. 124, No. 12, December, 1998. ©ASCE, ISSN 0733-9399/98/0012-1316-1324/\$8.00 + \$.50 per page. Paper No. 17980.

the variable spacing is twofold: (1) The variation of the compliances near the hole is quite abrupt; and (2) the plastic zone at the crack tip is too short to get resolved with a coarser spacing (but even for the fine spacing used, the plastic zone could not be resolved for thick plates).

Fig. 2(a) shows a few typical load-deflection diagrams plotted as $(\sigma_N - \sigma_e)/f_t'$ versus $(u - u_e)/G_f$, where u_e , σ_e are the load point deflection and nominal stress at the elastic limit, i.e., just before the cracks start to grow. These diagrams terminate at the maximum load state. The maximum load is calculated under the hypothesis that the initiation of the circumferential cracks immediately causes softening in the load-deflection di-

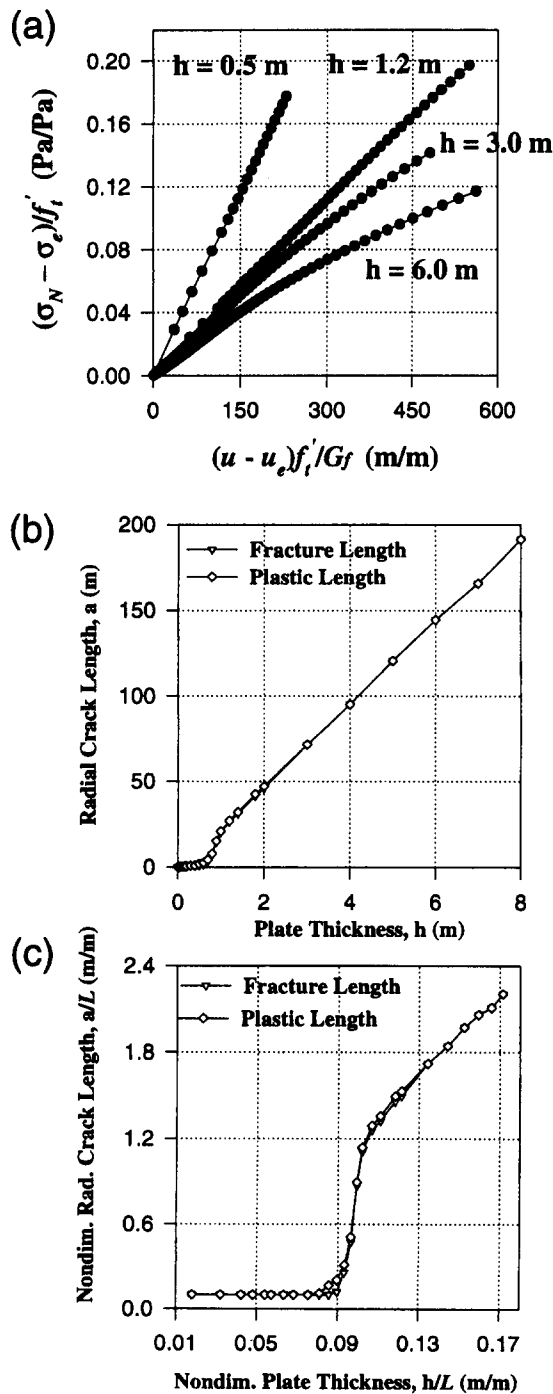


FIG. 2. Plot of: (a) Load-Displacement Diagrams for Plates of Various Thicknesses; (b) Calculated Radial Crack Length As Function of Plate Thickness; (c) Calculated Dimensionless Radial Crack Length As Function of Dimensionless Plate Thickness

agram. This hypothesis is based on the experimental observations of Frankenstein (1963). The calculated curves shown in Fig. 2(a) computationally verify the field test results obtained by Frankenstein (1963). However, even if the maximum load occurred only after some finite growth of the circumferential cracks, this hypothesis would be on the safe side.

Fig. 1 shows the distributions of stress σ_M due to bending moment, stress σ_N due to normal force, and crack depth $b(r)$ along the ray with the crack, calculated for various crack lengths a . The distributions for different loading phases differ. Initially, as the radial crack extends, σ_M and σ_N gradually increase from the first node to the end of the radial crack. Note that, behind the crack front, the bending moment is positive and the normal force is negative. The normal force at the tip of the radial crack is negligible. The crack depth gradually increases as the crack length increases, and the crack edge has a descending slope except near the hole when the crack gets long. As the radial crack becomes sufficiently long, the bending moment profile changes its shape from a gradually ascending profile to a valley-shaped profile with a high peak at the front. The peak would doubtless become a singularity if the plastic zone were negligible and if the nodal spacing approached zero. [Such singularities in the compliance function of a floating plate with many cracks were identified analytically by Dempsey et al. (1995a,b).] The normal force continuously increases behind the crack front. The contribution of the dome effect caused by partial opening of the crack can be judged by comparing the load-deflection diagrams.

When $\alpha \approx 0.4L$, σ_M at the first node is about $0.75L$ and σ_N is about $0.2L$. At that moment, as revealed by Fig. 1, the rate of the vertical crack growth with the radial crack length a slows down near the hole, but no crack unloading [stage 4, Fig. 2(d)] nor shortening (stage 5) ever occurs. The slowing of the vertical crack growth is caused by the development of significant compressive normal forces in the uncracked portion of the ice plate thickness. As the radial crack length reaches about $2.0L$, the vertical crack depth near the hole almost halts its growth and does not exceed the depth beyond about $0.8h$ as the radial crack length increases. The circumferential crack initiates from the radial crack when this limiting vertical crack depth is closely approached.

In the cracked ice plate, a part of the applied load is carried by in-plane normal forces, creating a sort of dome effect. The dome effect is characterized by the distance of the normal force resultant above the middle plane of the plate, which is $\delta(r) = -M(r)/N(r)$. Fig. 1 shows the profiles of $\delta(r)$ at various stages of loading. From these profiles we see that the surface of $\delta(r)$ does not have the simple shape of a dome, but is quite complicated, with positive and negative peaks near the radial crack front. The surface $\delta(r)$ is above the middle plane in the central portion of the plane where the normal compressive forces are high and greatly contribute to the load-carrying capacity. In the outer region, the surface is below the middle plane, but does not cause a significant reduction of load capacity of the plate because in that region the normal forces and bending moments are very small.

SIZE EFFECT AND INFLUENCING PARAMETERS

The size effect is understood as the size dependence of the nominal strength $\sigma_N = P_{\max}/h^2$ when geometrically similar structures are compared (P_{\max} = maximum load). Characterization of the size effect is the most important benefit of using fracture mechanics. Failures governed by criteria expressed solely in terms of stresses or strains exhibit no size effect (Bažant 1993; Bažant and Chen 1997; Bažant and Planas 1997); i.e., the nominal strength is independent of the structure size when geometrically similar situations are compared. Failures governed by energy criteria and described by fracture me-

chanics generally exhibit a strong size effect (Bažant and Chen 1997; Bažant and Planas 1998), provided that a macroscopically large crack develops prior to the maximum load, as is the case here. Stable formation of such a large crack before failure is typical for quasi brittle materials, that is, materials with a large fracture process zone at the front of a major crack. In view of the in-situ tests reported by Dempsey et al. (1995a,b), Mulmule et al. (1995), and Dempsey (1996), the sea ice on the scale of interest for the penetration problem must be considered to be a quasibrittle material.

The solution may be regarded as a functional relation among eight variables: σ_N , h , G_f , f'_i , E , ρ , ν , and a_0 . However, as already mentioned, the ratio a/a_0 , where a = crack length at breakthrough load P_{max} , may be assumed to be so large that the effect of the radius a_0 of the hole on P_{max} or σ_N is negligible. Furthermore, E , ρ , and ν influence only the elastic deformations of the plate-water system, which are fully characterized by a single parameter, the flexural wavelength L . Therefore, the solution must be given by some function Π of only five variables, $\Pi(\sigma_N, h, G_f, f'_i, L) = 0$.

Buckingham's Π -theorem of dimensional analysis (Barenblatt 1979) states that the solution must be reducible to a function of N_v independent dimensionless variables, where $N_v = N_{all} - N_{ind}$; N_{all} = number of all independent variables; and N_{ind} = number of variables with independent physical dimensions. Here we have $N_{all} = 5$ and $N_{ind} = 2$, with the independent physical dimensions being the length and the force. So $N_v = 5 - 2 = 3$. We may choose these variables as indicated in the following form of solution:

$$\frac{\sigma_N}{f'_i} = \Phi \left(\frac{h}{l_0}, \frac{l_1}{l_0} \right) \quad (1)$$

where Φ = some function; $l_0 = EG_f/f'_i{}^2 = K_c^2/f'_i{}^2$; and $l_1 = E/\rho \propto L^4/h^3$. Here $K_c = \sqrt{EG_f}$ = fracture toughness (critical stress intensity factor); l_0 = Irwin's (1958) characteristic size of the fracture process zone [introduced for concrete by Hillerborg et al. (1976)]; and l_1 = second independent length parameter. Note that the flexural wavelength $L = [l_1 h^3 / 12(1 - \nu^2)]^{1/4}$.

The foregoing analysis shows that the elastic properties and specific weight of water influence the solution only through the ratio l_1/l_0 . As for the fracture characteristics of ice, G_f and f'_i , they influence the solution only through the value of l_0 , but not individually. This means that the size effect curve of σ_N/f'_i versus h/l_0 has only one parameter, namely, l_1/l_0 .

A set of size effect curves for various values of l_1/l_0 will, therefore, characterize all the possible situations. This conclusion is very useful because the values of G_f as well as f'_i for sea ice exhibit tremendous statistical variability and depend strongly on temperature, salinity, and the size and spacing of voids and channels filled with brine. On the other hand, the value of ρ is a constant and the value of Young's modulus E of ice does not exhibit such a large statistical variability as G_f and f'_i .

The values of Young's modulus E measured by ultrasound range approximately from 4 GPa (5.8×10^5 psi) to 11 GPa (1.6×10^6 psi). Because of the rate effect (or creep), however, the effective E value for static loading is much smaller. In the present computations, the value of $E = 1$ GPa (1.45×10^5 psi), the same as considered by Evans (1971), was considered as the basic value.

According to the review by Sanderson (1988) and the data of Dempsey et al. (1995a,b), a representative value for the tensile strength f'_i of sea ice is 0.5 MPa (72.5 psi). The value of tensile strength, however, has only a minor effect because the plastic zone at the crack tip is, at maximum load, very small. The fracture toughness K_c is much more important.

Sanderson (1988, page 91), based on small-scale tests, re-

ports K_c -values ranging from 0.044 MPa m^{-3/2} to 0.115 MN m^{-3/2}. According to these data and the information from Urabe and Yoshitake (1981) and Weeks and Mellor (1984), the value $K_c = 0.1$ MN m^{-3/2} [the same as considered by Bažant (1992a,b)] was used in computations. With $E = 1$ GPa, the corresponding value of fracture energy is $G_f = 10$ N/m, which was used by Bažant (1992a,b). [For comparison, the thermodynamic surface Gibbs free energy of pure ice is about 0.1 N/m; Ketchum and Hobbs (1969)]. According to Dempsey (personal communication, 1997), the representative value of the fracture energy of sea ice is $G_f = 10$ –15 N/m.

A higher value of fracture energy is indicated by the size effect observed in the large-scale in-situ fracture tests of sea ice recently conducted on the Arctic Ocean near Resolute by Dempsey et al. (1995a,b). The reader is also referred to Mulmule et al. (1995). These tests involved floating notched square specimens of ice 1.8 m thick, with sides ranging from $D = 0.5$ m to $D = 80$ m, loaded horizontally by a flat jack inserted into the notch of length $0.3D$ at a distance $0.02D$ from the mouth. The size effect plot of the reported data closely approaches the linear elastic fracture mechanics (LEFM) asymptote of $-1/2$. Dempsey et al. (1995a,b) did not report the fracture energy, but its value can be easily figured out from the maximum load data they reported. To this end, one needs to fit the size effect law to their data, determine the location of the asymptote [as proposed by Bažant and Pfeiffer (1987) and explained in detail in Bažant and Planas (1997)], and use the formula for the stress intensity factor (Tada et al. 1985) for the type of specimen used in these large-scale in-situ tests. The calculation provides $K_c = 2.1$ MN m^{-3/2} and, for $E \approx 8.8$ GPa, $G_f = 520$ N/m. With $f'_i \approx 2$ MPa, the characteristic size is then $l_0 \approx 0.5$ m, and $l_1/l_0 \approx 1.8 \times 10^6$. These are the effective values for the whole thickness of ice whose temperature varies from about -20°C on top to about -1°C in contact with seawater.

The values of fracture energy of sea ice depend on its temperature and on the loading rate. They are also different for cracks that grow in the floating ice plate vertically (parallel to grains or columnar crystals, which is called the VH orientation) or horizontally (normal to the grains, which is called the HH orientation) (Mulmule and Dempsey 1997).

The values from Dempsey et al.'s tests near Resolute, however, are pertinent to horizontal propagation of a long full-through vertical crack. In our problem, the crack propagates mainly vertically, which doubtless causes the fracture process zone to be smaller than in Dempsey's tests, and thus the effective fracture energy to be lower. Also, the anisotropy of sea ice is likely to cause the effective fracture energy for vertical crack propagation to be less than that for horizontal propagation, because the fracture runs along, rather than across, the vertical hexagonal columnar crystals of sea ice and along, rather than across, the vertical brine channels. This gives another reason why the fracture energy for the penetration problem should be considered smaller than in Dempsey et al.'s tests near Resolute.

In view of the preceding discussion, the representative value of the characteristic size of the fracture process zone for the present computations is chosen as $l_0 = 0.25$ m, with the ratio $l_1/l_0 = 4.5 \times 10^5$. The size effect results for these parameters and for the failure mode with six cracks in a star pattern are shown by the data circles in the bilogarithmic plot in Fig. 3(a).

To obtain information on the effect of parameter l_1/l_0 , additional computations have been run for the value $l_1/l_0 = 3.9 \times 10^4$. These are shown by the data squares in Fig. 3(a). It is immediately apparent from this figure that the difference between the trends of the data circles and data squares is rather small. This is not surprising, since l_1 and l_0 differ by several orders of magnitude, which means that they can hardly interact. Therefore, the effect of parameter l_1/l_0 can be neglected.

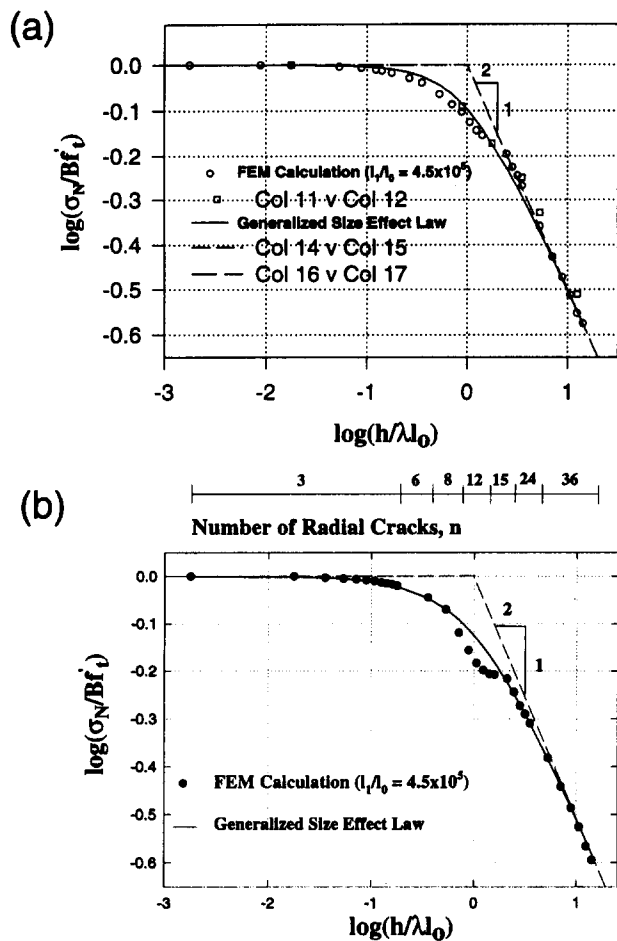


FIG. 3. Diagram of: (a) Size Effect Calculated for Fixed Number of Radial Cracks, $n = 6$; (b) Size Effect Calculated for Thickness Dependent Number of Radial Cracks Determined from Crack Initiation Analysis

(Values of $l_1/l_0 \geq 10^6$ have caused convergence problems, apparently because the fracture process zone in that case is too small to be resolved for large ice thicknesses by the assumed mesh.)

The calculated data circles in Fig. 3(a) trace a relatively smooth curve, except for a steep bump in the middle. This bump appears associated with the rapid rise in ratio a/h seen in Fig. 2(b,c), which occurs when h increases from 0.5 m to 1 m. For small thicknesses, approximately $h \leq 20$ cm, the radial crack length at maximum load remains approximately constant, which may be explained by the fact that the fracture process zone (or l_0) is not small compared to the plate thickness. In that case, the strength theory must be expected to apply, and indeed the size effect curve is initially horizontal. For thick plates, approximately for $h \geq 1$ m, the radial crack length at maximum load in Fig. 2(b,c) is approximately proportional to the flexural wavelength L (or to $h^{3/4}$). In that case, the quasibrittle size effect law should be followed, and it indeed is. If a/L did not approach a constant for thick enough plates, the size effect plot would not approach an asymptote of slope $-1/2$.

DEPENDENCE OF SIZE EFFECT ON NUMBER OF CRACKS

The dependence of the number of cracks on the plate thickness was studied in a second round of computations. For this purpose, one needs first to understand crack initiation from the smooth surface of the hole on which the vertical distributed load is assumed to be applied.

A simple method for determining the spacing of cracks ini-

tiating from the smooth surface of a half-space was proposed by Bažant et al. (1979) [see also Bažant and Cedolin (1991, section 12.6)] and was recently refined by Li and Bažant (1994) and Li et al. (1995). The method involves three conditions: (1) The stress before crack initiation attains the material tensile strength; (2) the energy release caused by the formation of cracks of finite initial length a_i is equal to the surface energy of these cracks determined from the fracture energy G_f of the material; and (3) the cracks of initial length a_i are in a critical state; i.e., their energy release rate is equal to G_f . These three conditions have also been applied by Li et al. (1995) to the crack spacing in highway pavements. The last two conditions imply the neglect of possible acoustic radiation of energy, and possible additional energy dissipation by distributed damage that is not included in G_f .

From the foregoing three conditions, one can determine the load level at which the initial cracks form, their initial length a_i , and their spacing. Li and Bažant (1994) deduced from these three conditions the number n_c of radial cracks initiating from a hole in the ice plate, as indicated in Table 1 of the companion paper; n_c increases from three cracks for ice plates under $0.1L$ thick, to 36 cracks for ice plates over $5L$ thick.

Taking the numbers of radial cracks for various ice thicknesses from the analysis of Li and Bažant (1994), and running the present computer program for each of these numbers, we obtain the size effect plot shown in Fig. 3(b). The numbers of radial cracks for various size ranges are indicated in the figure.

Comparing this figure with the previous Fig. 3(a) for $n_c = 6$, we see that the effect of the number of cracks is not strong (which is a similar conclusion to that of the plastic limit analysis of the penetration problem). The overall curvature of the size effect plot is only slightly less than in the previous case. The horizontal small-size asymptotic slope is slightly higher for the varying wedge angle analysis than for the constant angle analysis. The average slope between 0.001 m and 0.05 m plate thickness is 6.084×10^{-3} and 7.744×10^{-3} for Figs. 3(a) and 3(b), respectively, and the percent difference between the slopes is 0.21%. The large-size inclined asymptote, which has again the slope of $-1/2$, is slightly lower for the varying angle case than for the constant angle case. The slopes are 0.502 and 0.463 for Figs. 3(a) and 3(b), respectively, and the percent difference is 0.08%. The numerical results for varying numbers of cracks can again be closely described by Bažant's generalized size effect law in (2), in which $\lambda_0 = 2.55$, $m = 1/2$, $r = 1.2$, and $l_0 = 0.25$ m. This law is shown in Fig. 3(b) by the continuous curve.

ANALYSIS OF SIZE EFFECT RESULTS

The size effect was initially studied under the assumption of full-through bending cracks for which the large size behavior was found to be $\sigma_N \propto h^{-3/8}$, as confirmed by the studies of Slepyan (1990), Bažant (1992a,b), Bažant and Li (1994a,b), and Li and Bažant (1994). [For long full-through thermal bending cracks, a similar size effect was found by Bažant (1992a,b).] The reason why for full-through cracks the asymptotic size effect is not $\sigma_N \propto h^{-1/2}$ is because the plate thickness h is actually not a dimension in the plane (x, y) of the boundary value problem of the infinite floating plate, but merely a parameter giving the cylindrical stiffness D . No physical dimension in the plane (x, y) exists (except for the hole, whose effect is, however, considered negligible). The only dimension present is the flexural wavelength L , which depends on the thickness as $L \propto h^{3/4}$. Thus, for full-through fracture, the size effect must be expected in the form $\sigma_N \propto L^{-1/2}$, or $\sigma_N \propto (h^{3/4})^{-1/2} \propto h^{-3/8}$. This was evidenced by the penetration studies of Slepyan (1990), Bažant (1992a,b), Bažant and Li (1994a,b), and Li and Bažant (1994) [and for thermal fracture, Bažant (1992a,b)].

A different asymptotic size effect, however, is exhibited by the present numerical solution. As seen in Figs. 3(a) and 3(b), the large-size asymptote of the size effect curve has the slope $-1/2$, i.e., $\sigma_N \propto h^{-1/2}$ for $h \rightarrow \infty$, which is the standard asymptotic size effect. The reason why the asymptotic size effect $\sigma_N \propto h^{-3/8}$ does not apply is because the crack is not full-through, but is growing across the plate thickness, which is a standard crack propagation problem. Even though the numerical solution is two-dimensional (in the horizontal plane), the fracture propagates only in the third dimension and its behavior is embedded in the Rice-Levy springs. An interesting theoretical question is whether the (3/8)-power law for full-through cracks can be obtained as a limiting case of the present solution. The answer is no, because the Rice-Levy springs cannot simulate the conditions at the tip of a horizontally propagating full-through bending crack.

In a recent simplified solution of Dempsey et al. (1995a,b), in which the depth of part-through cracks was assumed to be constant over the entire crack length, the ice was assumed to follow LEFM, and the case of many cracks was considered, the size effect was of the type $\sigma_N \propto h^{-1/2}$ for all h .

As is typical of quasi brittle fracture (Bažant 1984; Bažant and Chen 1997; Bažant and Planas 1998), the small-size asymptote of the calculated size effect plot in Fig. 3(a) is horizontal and corresponds to a solution according to plastic limit analysis (strength theory), whose applications to the penetration problem were reviewed by Kerr (1996) [see also Sodhi (1995a,b, 1996)]. The present computations show that plastic limit analysis (strength theory) corresponding to the horizontal asymptote of the size effect plot, is a good enough approximation only for ice thicknesses up to about 0.2 m (assuming that $l_0 = 0.25$ m). At the same time, the σ_N values for the horizontal asymptote can scatter widely, depending on the type of ice and the environmental conditions (air and water temperature). This may explain why no size effect was observed in small-scale laboratory experiments.

The large-size asymptote of the size effect plot, which has the slope of $-1/2$ corresponding to LEFM, is seen to be a good enough approximation for ice thicknesses over 1.0 m. The value of parameter λ_0 is chosen so that $h = \lambda_0 l_0$ would represent the thickness at the intersection point of the two asymptotes. From the present numerical results, $\lambda_0 = 2.26$. The ratio $\beta = h/(\lambda_0 l_0)$ determined in this manner has been called the brittleness number (Bažant 1987; Bažant and Pfeiffer 1987; Bažant and Planas 1997). The limit $\beta \rightarrow \infty$ indicates the perfectly brittle response, i.e., LEFM, and the limit $\beta \rightarrow 0$ indicates the perfectly ductile (plastic) response.

The present numerical results, spanning over four orders of magnitude of ice thickness, can be closely fitted by the generalized form of Bažant's size effect law (Bažant 1985; Bažant and Pfeiffer 1987; Bažant and Chen 1997; Bažant and Planas 1998), shown by the continuous curve in Fig. 3(a)

$$\frac{\sigma_N}{Bf'_i} = \left[1 + \left(\frac{h}{\lambda_0 l_0} \right)^r \right]^{-1/2r} \quad (2)$$

Here, the dimensionless parameters found by fitting of the numerical results are $B = 1.214$; $\lambda_0 = 2.55$; $m = 1/2$; $r = 1.55$; the dimensional parameters used in Fig. 3 are $l_0 = 0.25$ m; and $f'_i = 0.2$ MPa (from which $K_c = f'_i \sqrt{l_0} = 0.1$ MN m $^{-3/2}$). This approximate law has been derived as the asymptotic matching between the large-size and small-size expansions of the size effect (Bažant 1995a,b, 1997).

Eq. (1) can be written as $Y = AX + C$, where $X = h^r$, $Y = (\sigma_N)^{-2r}$, $A = (Bf'_i)^{-2r}$, and $C = 1/(\lambda_0 l_0 B f'_i)^{2r}$. This means that, if r is known, the values of Bf'_i and $\lambda_0 l_0$ can be determined by linear regression. The regression may be conducted for various chosen r values such that the optimum r is found.

With the aforementioned dimensionless values of B , λ , m ,

and r , (2) can be used as a general approximate prediction formula, provided, of course, the values of l_0 and f'_i are known.

The present numerical results confirm that the (3/8)-power law previously obtained for full-through cracks is not applicable. The (3/8)-power law would apply when the horizontal forces are sufficiently small compared to the bending moments. This would have to happen for a floating plate that is sufficiently thin and sufficiently fragile so as to fail by fracture rather than by plastic yielding. Such conditions may be expected to occur when $l_0 \ll h \ll L$. But this does not occur in the realistic range of ice properties.

The (3/8)-power law does, nevertheless, apply to the scaling of the critical temperature difference that can produce long thermal fractures running in a stationary state, analyzed by Bažant (1992a,b). The reason is that, despite the presence of a large fracture process zone with a part-through crack, there exists around the front of a long enough crack a control region that moves with the crack front, remains in a stationary state, and is so large that ahead of this region there is no deflection and no damage, while behind this region there is a full-through crack if the crack is long.

Another interesting plot is that of the radial crack length a versus ice thickness h , shown in Fig. 2(b). Two values of a are shown: the length to the front of the plastic zone at the bottom surface of the plate, and the length to the front of the open LEFM crack. As can be seen, both crack lengths are very close and are undistinguishable for large thicknesses. This means that the plastic behavior is not important for the overall response, and confirms that a very accurate but complex modeling of the plastic zone at the crack front is not necessary. The reason that no plastic crack length is seen in Fig. 2(b) for large plate thicknesses is that the nodal spacing is increased in proportion to the ice thickness. For thick plates the nodal spacing becomes larger than the length of the plastic zone. This is clear from Fig. 2(c), showing the dimensionless crack length a/L versus dimensionless ice thickness h/L .

COMPARISONS WITH TEST DATA

The present results on the number of cracks roughly agree with the field observations of Frankenstein (1963, 1966) and Lichtenberger et al. (1974). Frankenstein made extensive observations on lake ice, which can be assumed to behave similarly as sea ice. Despite irregularities in the observed crack patterns, Frankenstein's tests clearly show that the number n_c of cracks increases with the ice thickness h .

The aforementioned experimental data on the size effect in penetration of sea ice were analyzed by Sodhi (1995a,b, 1996) under the assumption that sea ice is a plastic material. Sodhi concluded that these data confirm the absence of size effect, which is characteristic of his solution based on plasticity.

However, this conclusion is due solely to a questionable statistical treatment of the data. Sodhi (1995a) based his conclusion on the plot of P_{\max} versus h , as shown in Fig. 4(a). This kind of plot seems, indeed, to suggest that P_{\max} is approximately proportional to h^2 , which would mean that σ_N is constant, free of size effect. However, such a way of reasoning is deceptive. The main reason is that, implicitly, a strong deterministic variation obscuring the size effect, namely, the proportionality of P_{\max} to h^2 , has been superposed on the test data by Sodhi's choice of coordinates of the plot.

What a misleading effect such a choice of coordinates can have is illustrated in Figs. 4(b and c). In Fig. 4(b), we assume hypothetical perfect data, conforming exactly to Bažant's size effect law. Then we plot the same data in the graph of $\log P_{\max}$ versus $\log h$ [Fig. 4(c)]. According to Sodhi's viewpoint that there is no size effect, one would pass the regression line of slope 2 shown in the figure. The comparison of this regression line with the data seems now acceptable, indicating

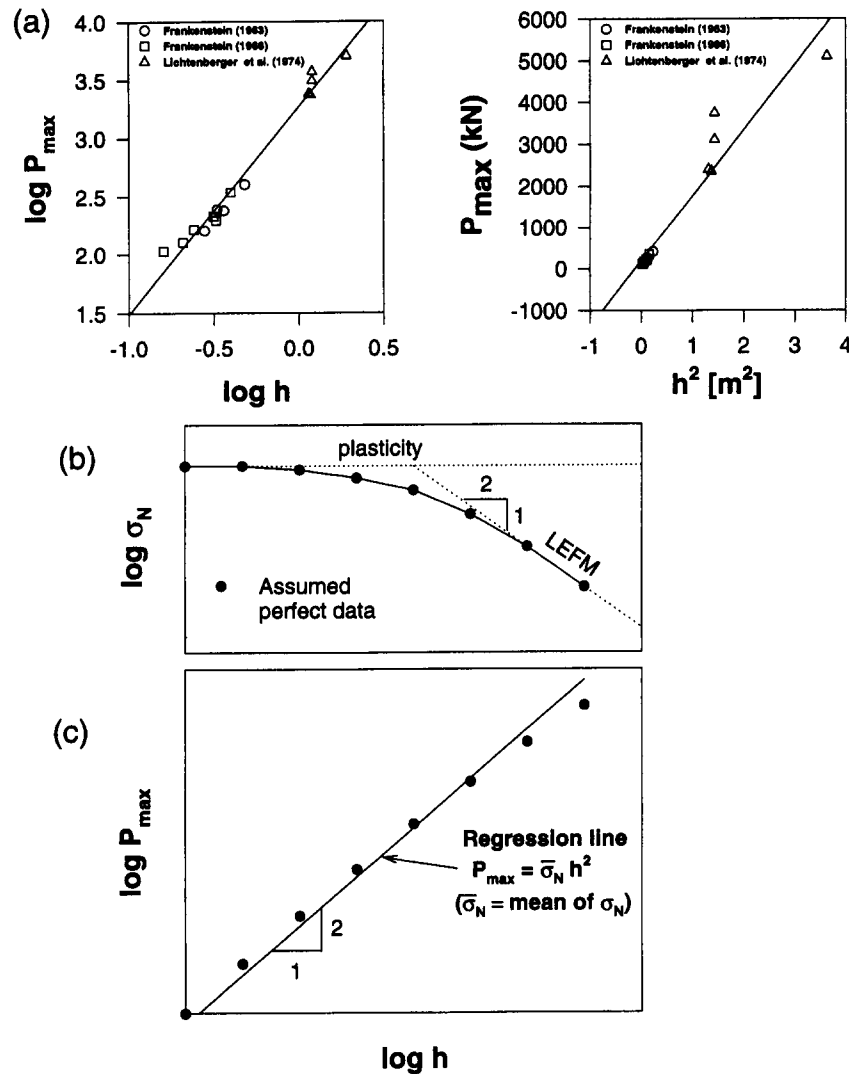


FIG. 4. Diagram of: (a) Sodhi's Way of Plotting Existing Test Data; (b) Incorrect Choice of Coordinates for Statistical Analysis; (c) Incorrect Choice of Coordinates for Statistical Analysis

a relatively low coefficient of variation of the deviations from the regression line. The comparison would look even more acceptable if the inevitable random scatter were superposed. Yet this is the case of perfect agreement with the size effect law.

A second questionable aspect of Sodhi's (1995a,b) evaluation of test data is that he correlated in the same diagram the test results from different test series while implying the same ice properties. However, the ice properties were most likely quite different. If the differences in ice properties among the two test series of Frankenstein (1963, 1966) and that of Lichtenberger et al. (1974) were taken into account, the groups of data points for these tests could shift vertically in the plot in Fig. 4(a). Thus, what looks like a good agreement with the proportionality of P_{\max} to h^2 could be lost by such vertical shifts. It is probably by chance that the differences among the ice properties compensated for the size effect.

Since the size effect is the deviation from the proportionality of P to h^2 , the only nonobfuscating way that can bring the size effect to light is to plot the values of $\sigma_N = P/h^2$; i.e., to construct the plot of the measured values of $\log \sigma_N = \log(P/h^2)$ versus $\log h$ (rather than a plot of P versus h). Because the ice properties in different test series were not the same, the plots intended to check for size effect should be made separately for each test series. This is done in Fig. 5(a) for the

three data series reported by Frankenstein (1963, 1966) and Lichtenberger et al. (1974). Looking at these plots now leads to a conclusion very different from Sodhi's: There is a clear size effect in each test series.

Furthermore, Fig. 5(b) shows the linear regression plots of $1/\sigma_N^2$ versus h , in which the size effect law (2) with $r = 1$ is represented by the regression line. These linear regression plots make it possible to determine the coefficients of variation of the slope of the regression line. However, the data are too few and the size range too narrow to obtain meaningful statistics.

Finally, Fig. 5(c) shows all three data sets in one plot of $\log(\sigma_N/Bf'_i)$ versus $\log(h/\lambda_0 l_0)$, and in another plot of $(Bf'_i/\sigma_N)^2$ versus $h/\lambda_0 l_0$. These unified plots use the optimum values of Bf'_i and $\lambda_0 l_0$ obtained by a previous separate regression of each data set. These two plots [Fig. 5(c)] confirm that the present theory is in overall acceptable agreement with the available test results.

In view of the high scatter and limited size range of the available data, it cannot be claimed, however, that the existing test results actually prove the present theory. There might exist another theory that fits these limited data also. The answer to this question and the verification for large ice thicknesses will have to await measurements of a much broader size range. Nevertheless, all the plots in Fig. 5 visually demonstrate the invalidity of Sodhi's claim that there is no size effect.

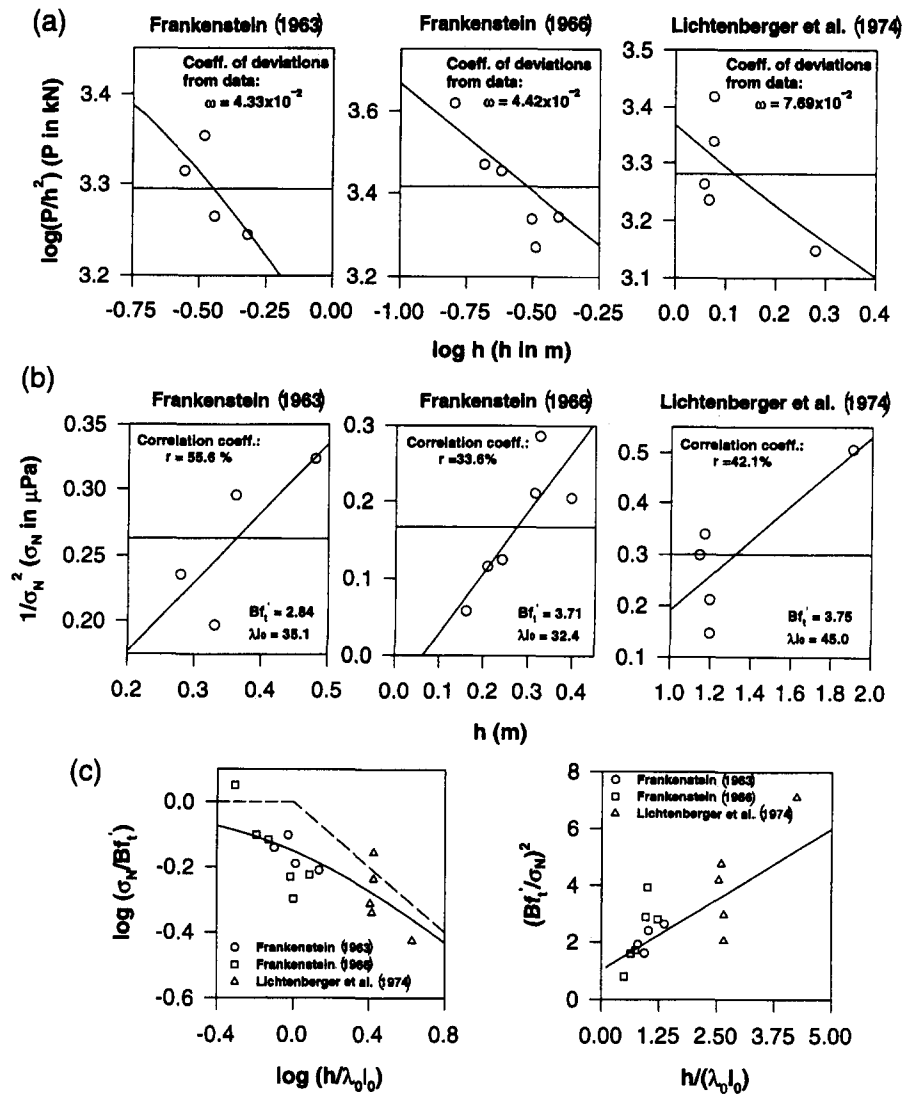


FIG. 5. Comparison of Present Theory with Test Data from Literature

SOME REMAINING QUESTIONS

Although the present study probably answers the main questions in the ice penetration problem, several questions still remain. Due to temperature variations through the ice plate and diffusion of brine, the ice plate is not homogeneous. Its bottom, where the temperature is near the melting point, is very soft and weak, while the top is cold and thus stiff and strong. The present analysis must be interpreted in the sense of a certain effective ice thickness that gives about the same bending stiffness as that of the actual ice plate, and the values of K_f , f_i' , and E must be interpreted as the equivalent effective properties throughout the thickness. An accurate analysis, however, would have to take these differences into account.

Another question is the neglect of the rate of loading. Sea ice exhibits creep, and the effective fracture energy as well as the strength depend on the rate of crack growth. Regarding the number of cracks, there is another phenomenon that may play a role. It could happen that some of the radial cracks could grow longer than others. A bifurcation of the equilibrium path, in which a bifurcated solution with unequal crack lengths may be followed, is a possibility. This problem could be analyzed similarly to the problem of bifurcation and changes of spacing in the evolution of a system of parallel cooling cracks in a half-space (Bažant et al. 1979; Bažant and Cedolin 1991, section 12.6). Analysis of this problem would require abandoning the present assumption of symmetry of response.

Finally, the value of l_0 might be larger for a thicker ice plate, because of its higher heterogeneity.

CONCLUSIONS

1. The mechanism of penetration of a floating sea ice plate involves the growth of radial cracks that cut only through a part of the ice thickness. The crack depth at maximum load is about 80% of the ice thickness.
2. The nominal strength of the sea ice plate exhibits a strong size effect. For small ice thicknesses (up to about 0.2 m), the size effect can be neglected. For large thicknesses (exceeding about 1 m), the logarithmic size effect plot approaches an asymptote of slope $-1/2$, which is typical of LEFM. The previously derived asymptote of slope $-3/8$, which corresponds to full-through cracks, cannot occur for realistic properties of sea ice.
3. The characteristics of an effective numerical model are as follows: (1) The cracked radial section is subdivided into vertical strips in which the crack is assumed to grow upward, independently of the cracks in the adjacent strips; (2) the cracked vertical strip is modeled by the Rice-Levy nonlinear softening line spring; (3) a yield criterion is adopted to decide crack initiation in the vertical strips, and the initial plastic crack growth follows a nonassociated LEFM flow rule; (4) compliance matrices are used to characterize the uncracked sector of the ice

plate on the elastic foundation; (5) the Levenberg-Marquardt nonlinear optimization algorithm is used to solve a large system of nonlinear equations based on the initial estimate provided by the solution of the previous loading step; and (6) the maximum load is calculated under the assumption that the initiation of the circumferential cracks immediately causes softening in the load-deflection diagram.

4. The previously established dependence of the number of radial cracks on the ice thickness does not have a strong influence on the size effect plot.
5. Dimensional analysis shows that, with some mild simplifications, the dimensionless nominal strength of the plate depends on only two parameters—the dimensionless size and the dimensionless elastic modulus of ice. The latter is further shown to have little influence. Consequently, one dimensionless size effect curve can approximate the response in general.
6. The existing field measurements of size effect agree with the present theory well, although their size range is too limited for actually proving the theory. Sodhi's opinion that there is no size effect is invalid for ice plates thicker than about 20 cm.
7. Until calibration by more extensive test data becomes possible, based on (1) it is recommended to predict the static load capacity of the sea ice plate from Fig. 3(b) or, approximately, from the formula

$$P_{\max} = \frac{1.214f_i h^2}{[1 + (h/2.55l_0)^{1.55}]^{1/3.1}}$$

APPENDIX I. LEVENBERG-MARQUARDT NONLINEAR OPTIMIZATION ALGORITHM

The Levenberg-Marquardt iterative algorithm (Levenberg 1944; Marquardt 1963) combines the best features of the inverse-Hessian method and the steepest descent method to minimize the sum of squares of m nonlinear functions f_i on n -dimensional vector \mathbf{x} (column matrix); $\mathbf{f}^2(\mathbf{x}) = \sum_{i=1}^m f_i^2(\mathbf{x}) = \min$. In the initial iterations, when the trial values are not close to the solution, the steepest descent method (or gradient method) is used

$$\mathbf{x}_{\text{next}} = \mathbf{x}_{\text{trial}} - \text{const.} \times \nabla \mathbf{f}^2(\mathbf{x}) \quad (3)$$

where \mathbf{f} = column matrix of components f_i , and the constant must be chosen small enough. In proximity of the correct solution, the inverse-Hessian method is used to converge rapidly to the best estimate

$$\mathbf{x}_{\text{best}} = \mathbf{x}_{\text{trial}} + \mathbf{H}^{-1}[-\nabla \mathbf{f}^2(\mathbf{x})] \quad (4)$$

where \mathbf{H} = Hessian matrix whose components are the second partial derivatives of the function. To judge the accuracy, the algorithm also calculates the standard deviations of the initial guess of the solution and of the final solution.

ACKNOWLEDGMENTS

Financial support under grant N00014-91-J-1109 (monitored by Dr. Y. Rajapakse) from the Office of Naval Research to Northwestern University is gratefully acknowledged.

APPENDIX II. REFERENCES

- Barenblatt, G. I. (1979). *Similarity, self-similarity and intermediate asymptotics*. Consultants Bureau, New York.
- Bažant, Z. P. (1984). "Size effect in blunt fracture: Concrete, rock, and metal." *J. Engrg. Mech.*, ASCE, 110, 518–535.
- Bažant, Z. P. (1985). "Fracture mechanics and strain-softening in concrete." *U.S.-Japan Seminar on Finite Element Anal. of Reinforced Concrete Struct.*, Preprints, 1, 47–69.
- Bažant, Z. P. (1992a). "Large-scale fracture of sea ice plates." *Proc., 11th IAHR Ice Symp.*, T. M. Hruday, ed., IAHR, Delft, The Netherlands, 2, 991–1005 (held in Banff, Canada).
- Bažant, Z. P. (1992b). "Large-scale thermal bending fracture of sea ice plate." *J. Geophys. Res.—Oc.*, 97(C11), 17739–17751.
- Bažant, Z. P. (1993). "Scaling laws in mechanics of failure." *J. Engrg. Mech.*, 119(9), 1828–1844.
- Bažant, Z. P. (1995a). "Scaling of quasibrittle fracture and the fractal question." *J. Mat. and Technol.*, 117(Oct.), 361–367.
- Bažant, Z. P. (1995b). "Scaling theories for quasibrittle fracture: Recent advances and new directions." *Fracture mechanics of concrete structures. Proc., 2nd Int. Conf. on Fracture Mech. of Concrete and Concrete Struct. FraMCoS-2*, F. H. Wittmann, ed., Aedificatio Publishers, Freiburg, Germany, 515–534 (held at ETH, Zürich).
- Bažant, Z. P. (1997). "Scaling of quasibrittle fracture: Asymptotic analysis." *Int. J. Fracture*, 83(1), 19–40.
- Bažant, Z. P., and Cedolin, L. (1991). *Stability of structures: Elastic, inelastic, fracture and damage theories*. Oxford University Press, New York.
- Bažant, Z. P., and Chen, E.-P. (1997). "Scaling of structural failure." *Appl. Mech. Rev.*, 50(10), 593–627.
- Bažant, Z. P., and Kim, J. J. H. (1998). "Size effect in penetration of sea ice plate with part-through cracks. I: Theory." *J. Engrg. Mech.*, ASCE, 124(12), 1310–1315.
- Bažant, Z. P., and Li, Y.-N. (1994a). "Penetration fracture of sea ice plate: Simplified analysis and size effect." *J. Engrg. Mech.*, ASCE, 120(6), 1304–1321.
- Bažant, Z. P., and Li, Y.-N. (1994b). "Penetration through floating sea ice plate and size effect: Simplified fracture analysis." *J. Engrg. Mech.*, ASCE, 120(7), 1304–1321.
- Bažant, Z. P., Ohtsubo, R., and Aoh, K. (1979). "Stability and post-critical growth of a system of cooling and shrinkage cracks." *Int. J. Fracture*, 15, 443–456.
- Bažant, Z. P., and Pfeiffer, P. A. (1987). "Determination of fracture energy from size effect and brittleness number." *ACI Mat. J.*, 84, 463–480.
- Bažant, Z. P., and Planas, J. (1998). *Fracture and size effect in concrete and other quasibrittle materials*. CRC Press, Boca Raton, Fla.
- Dempsey, J. P. (1996). "Scale effects on the fracture of ice." *The Johannes Weertmann Symp.*, R. J. Arsenault et al., eds., The Minerals, Metals and Mat. Soc. (TMS), Warrendale, Pa., 351–361.
- Dempsey, J. P., Adamson, R. M., and Mulmule, S. V. (1995a). "Large-scale in-situ fracture of ice." *Proc. FraMCoS-2*, F. H. Wittmann, ed., Aedificatio Publishers, D-79104, Freiburg, Germany (held in Zürich).
- Dempsey, J. P., Slepnyan, L. I., and Shekhtman, I. I. (1995b). "Radial cracking with closure." *Int. J. Fracture*, 73(3), 233–261.
- Frankenstein, E. G. (1963). "Load test data for lake ice sheet." *Tech. Rep. 89*, U.S. Army Cold Regions Res. and Engrg. Lab., Hanover, N.H.
- Frankenstein, E. G. (1966). "Strength of ice sheets." *Proc., Conf. on Ice Pressures against Struct., Tech. Memorandum No. 92, NRCC No. 9851*, Laval Univ., Québec, PQ, Nat. Res. Council of Canada, 79–87.
- Hillerborg, A., Modéer, M., and Petersson, P. E. (1976). "Analysis of crack formation and crack growth in concrete by means of fracture mechanics and finite elements." *Cement and Concrete Res.*, 6, 773–782.
- Kerr, A. D. (1996). "Bearing capacity of floating ice covers subjected to static, moving, and oscillatory loads." *Appl. Mech. Rev.*, 49(11), 463–476.
- Levenberg, K. (1944). "A method for the solution of certain nonlinear problems in least-squares." *Quarterly Appl. Mathematics*, 2, 164–168.
- Li, Y.-N., and Bažant, Z. P. (1994). "Penetration fracture of sea ice plate: 2D analysis and size effect." *J. Engrg. Mech.*, ASCE, 120(7), 1481–1498.
- Li, Y.-N., Hong, A. N., and Bažant, Z. P. (1995). "Initiation of parallel cracks from surface of elastic half-plane." *Int. J. Fracture*, 69, 357–369.
- Lichtenberger, G. J., Jones, J. W., Stegall, R. D., and Zadow, D. W. (1974). "Static ice loading tests, Resolute Bay—Winter 1973/74." *APOA Proj. No. 64, Rep. 745B-74-14 (CREEL Bib. No. 34-3095)*, Sunoco Sci. and Technol., Richardson, Tex.
- Marquardt, D. W. (1963). "An algorithm for least-squares estimation of nonlinear parameters." *J. Soc. Industrial Appl. Mathematics*, 11, 431–441.
- Mulmule, S. V., and Dempsey, J. P. (1997). "Stress-separation curves for saline ice using fictitious crack model." *J. Engrg. Mech.*, ASCE, 123(8), 870–877.
- Mulmule, S. V., Dempsey, J. P., and Adamson, R. M. (1995). "Large-

- scale in-situ ice fracture experiments—Part II: Modeling aspects.” *Ice mechanics—1995*, J. P. Dempsey and Y. Rajapakse, eds., ASCE AMD, New York, 207, 129–146.
- Sanderson, T. J. O. (1988). *Ice mechanics: Risks to offshore structures*. Graham and Trotman Limited, London.
- Sodhi, D. S. (1995a). “Breakthrough loads of floating ice sheets.” *J. Cold Reg. Engrg.*, ASCE, 9(1), 4–20.
- Sodhi, D. S. (1995b). “Wedging action during vertical penetration of floating ice sheets.” *Ice mechanics—1995*, J. P. Dempsey and Y. Rajapakse, eds., ASME AMD, New York, 207, 65–80.
- Sodhi, D. S. (1996). “Deflection analysis of radially cracked floating ice sheets.” *17th Int. Conf. OMAE Proc., Book No. G00954*, 97–101.
- Tada, H., Paris, P. C., and Irwin, G. R. (1985). *Stress analysis of cracks handbook*. Del Research Corp., Hellertown, Pa.